

Article

Prediction of Resistance Spot Weld Quality of 780 MPa Grade Steel Using Adaptive Resonance Theory Artificial Neural Networks

Insung Hwang¹, Hyeonsang Yun¹, Jinyoung Yoon^{1,2}, Munjin Kang¹, Dongcheol Kim¹ and Young-Min Kim^{1,*} 

¹ Joining R&D Group, Korea Institute of Industrial Technology, 156 Gaetbeol-ro (Songdo-dong), Yeonsu-Gu, Incheon 21999, Korea; hisman@kitech.re.kr (I.H.); losineil@gmail.com (H.Y.); 0521jin@kitech.re.kr (J.Y.); moonjin@kitech.re.kr (M.K.); dckim@kitech.re.kr (D.K.)

² School of Mechanical Engineering, Hanyang University, 222 Wangsimni-ro, Seoul 04763, Korea

* Correspondence: ymkim77@kitech.re.kr; Tel.: +82-32-850-0232

Received: 31 May 2018; Accepted: 12 June 2018; Published: 13 June 2018



Abstract: In this study, the weld quality of 780 MPa grade dual phase (DP) steel with 1.0 mm thickness was predicted using adaptive resonance theory (ART) artificial neural networks. The welding voltage and current signals measured during resistance spot welding (RSW) were used as the input layer data, and the tensile shear strength, nugget size, and fracture shape of the weld were used as the output layer data. The learning was performed by the ART artificial neural networks using the input layer and output layer data, and the patterns of learning result were classified by the setting of vigilance parameter, ρ . When the vigilance parameter is 0.8, the best-predicted results were obtained for the tensile shear strength, nugget size, and fracture shape of welds.

Keywords: adaptive resonance theory; artificial neural networks; resistance spot welding; weld quality

1. Introduction

Recently, there has been an increasing demand for lightweight automobiles to improve fuel efficiency worldwide, and regulations for crashworthiness are being strengthened [1,2]. In order to enhance the crashworthiness, the thickness of the material for the automobile's body must be increased. However, as the thickness increases, the effect of weight reduction is reduced. Therefore, studies have been carried out to obtain the crashworthiness and the effect of weight reduction, simultaneously. As a result, the application of advanced high strength steel (AHSS, 590–780 MPa grade) or ultra-high strength steel (UHSS, 980 MPa grade or more) has been expanded for automobile body materials. To increase the strength of high strength steel (HSS), many alloying elements are added or a heat treatment process is performed during the cooling process [3–6].

There are various methods of joining automobile bodies for weight reduction of automobiles, such as fusion welding, mechanical fastening (clinching, riveting), and adhesive bonding [7,8]. The resistance spot welding (RSW) is one of the effective welding methods of joining HSS for automobiles. The RSW of HSS is likely to cause expulsion easily due to high resistivity, and the range of appropriate welding conditions, such as welding current, welding time and electrode force, tends to be very narrow. In general, the welding quality in RSW can be expressed in terms of strength (tensile shear strength or cross tensile strength), nugget size, or fracture mode (interfacial fracture or pull-out fracture). Many studies have been carried out on the welding quality in RSW. Ramazani et al. [9] presented the characterization and mechanical properties of the spot welded dual phase (DP) 600 steel under fixed welding condition. Jia et al. [10] investigated the microstructure, tensile shear strength,

nugget size and failure mode of resistance spot welded 0.1C–5Mn steel under the various welding currents and times. Spena et al. [11] reported the welding current and time are the main factors affecting the shear strength of galvanized quenching and partitioning (Q&P) and transformation induced plasticity (TRIP) steel spot welds, and electrode force is a minor factor. Also, the author reported the electrode force has a beneficial effect on corrosion resistance of the internal side of the spot welds. Tutar et al. [12] evaluated the effect of the weld current on the microstructure and mechanical properties of spot welded twinning-induced plasticity (TWIP) steel sheet. The higher welding currents accelerated the formation of a macro expulsion cavity in the fusion zone and no strong relationship was between the hardness in the weld zone and the welding current. Chabok et al. [13] reported the microstructural evolution of resistance spot welded 1000 MPa DP steel under single pulse weld and double pulse weld, and mechanical properties and failure mechanisms. And cross-tension strength under a double pulse weld scheme was higher than that under a single pulse weld scheme. It is very important to predict weld quality in real time by inspecting the weld in a short time during welding process or immediately after welding. There are several previous kinds of research to examine or predict weld quality using various methods. Chen et al. [14] measured the nugget size of the weld using an ultrasonic sensor. However, using an ultrasonic sensor, there is a possibility that an error of the measurement value may occur due to the change of the weld shape depending on the indentation depth of the welds. Lee et al. [15] measured the temperature distribution of the material surface around the electrodes using a thermal imaging camera and evaluated the weld quality. In addition, there is a study that estimates the weld quality by measuring the expansion and contraction behavior of the weld nugget using a displacement sensor [16]. In these methods mentioned above, the prediction result may vary depending on the thickness or the kind of the material, and the prediction error due to the contamination or deterioration of the sensor may be largely generated.

On the other hand, in the RSW, the welding voltage and current signal affect the amount of heat input to the material and the welding quality. Therefore, some research on the welding quality monitoring using the welding voltage and current signal have been recently reported. El-Banna et al. [17] proposed a model that predicts the size of welding nugget and the occurrence of expulsion through learning vector quantization (LVQ) artificial neural network using input layer parameters such as maximum value, minimum value, standard deviation, and slope of dynamic resistance extracted from dynamic resistance pattern of RSW. In the study of Zhao et al. [18], a graph of the voltage-current (U-I image) was drawn using the welding voltage and current signal of RSW. In this paper, a model was proposed for determining the nugget size and the occurrence of expulsion by applying artificial neural network using the shape information of the graph as input layer parameter. Kim et al. [19] showed that the adaptive resonance theory ART neural network can be used to classify the dynamic resistance signals of RSW into six patterns, and the correlation between these patterns and the tensile shear strength of the weld was investigated. Also, it was confirmed that the pattern satisfying the required strength is classified according to the shape of six kinds of dynamic resistance patterns.

It is very important to predict the weld quality of RSW with high accuracy in real time. Recently, along with the remarkable advancement of computer performance, a technology for accurately predicting natural phenomena using an ART has greatly advanced. In particular, when a prediction model was made by inputting the new learning data, ART artificial neural networks have the advantage of learning based on existing learning models, unlike other artificial neural network prediction methods.

The purpose of this study is to predict the welding quality using ART artificial neural networks and verify the prediction accuracy through comparison with experimental data. The welding voltage and current signal measured during RSW were used as the input layer data, and the tensile strength, nugget size, and fracture shape of the weld were used as the information of the output layer. Learning of ART artificial neural networks was performed using the input layer signals and the output layer information, and patterns were classified according to the similar level of each output layer information

based on the learning results. Using the obtained learning model, the accuracy of the prediction for the new input layer data was verified quantitatively.

2. Experimental Procedures

2.1. Base Materials, Welding Equipment, and Conditions

The base material used in this study is the 780 MPa grade dual phase (DP) steel with the 1.0 mm thickness. The chemical compositions and the mechanical properties of the base material are given in Table 1. Figure 1 shows the shape of the base material used in the RSW experiment produced according to the standards of the American Welding Society (AWS D8.9M:2012) [20]. The RSW system used in this study is composed of a power supply, a servo welding gun and medium frequency direct current (MFDC) transformer with built-in welding voltage and current sensor. The power supply used was an inverter-controlled power supply that has a rated output current of 400 A and controls power at a switching frequency of 1 kHz. As the MFDC transformer, a transformer capable of converting a power-controlled alternative current (AC) voltage and current signal with a switching frequency of 1 kHz to a power conversion ratio of 50:1 was used. The servo welding gun was used with a maximum pressure of 400 kg_f.

Table 1. Chemical composition and mechanical properties of base material used in this study.

Chemical Composition (wt. %)						Mechanical Properties		
C	Si	Mn	P	S	Fe	Tensile Strength (MPa)	Yield Strength (MPa)	Elongation (%)
0.073	0.996	2.271	0.01	0.001	Bal.	813	508	21

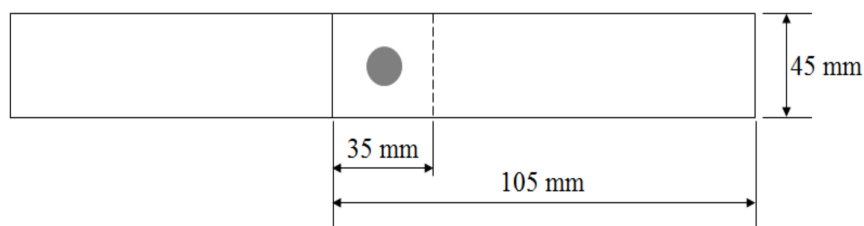


Figure 1. The shape of specimen for resistance spot welding.

The welding electrode used was a dome type electrode with an electrode diameter of 16 mm and a radius of 40 mm and a face diameter of 6 mm, as shown in Figure 2. Table 2 shows the welding conditions used for learning the tensile shear strength, nugget size, and fracture shape of resistance spot welds using the ART artificial neural network. In the field of automobile production, welding time of 333 ms or less is mainly used because productivity is emphasized in the field. Therefore, in this study, 167, 250, and 333 ms were selected as the welding time. Four experiments were conducted under the same conditions to reduce the error of the experiment. Three of these specimens were used in the tensile test and one was used to measure the nugget size.

Table 2. Welding conditions used in this study.

Welding Current (kA)	Welding Time (ms)	Electrode Force (kg _f)
4.0, 5.0, 6.0, 7.0	167, 250, 333	300



Figure 2. The shape of Cr–Cu electrode for resistance spot welding.

2.2. Measurement of the Welding Voltage and Current Signal

In order to measure the welding voltage and current signal for learning of input layer and verification of the output layer of ART artificial neural network, the welding voltage signal at the center position of the electrode was measured, and the welding current signal was measured by a hole sensor attached to the arm of the servo welding gun. The sampling rate of each signal is 50,000 samples/s. The average values of every 50 signals are calculated considering the switching frequency of 1 kHz. It means that average values of welding voltage and current signal per 1 ms were calculated. These average values were used as input layer signal parameters of the ART artificial neural network.

2.3. Evaluation of the Weld Quality

The tensile shear strength, nugget size, and fracture shape of weld were used for learning and verification of the output layer of ART artificial neural network. A universal testing machine with a maximum load of 5 tons was used for measuring the tensile shear strength of welds at the tensile test speed of 10 mm/min according to the standards of the American Welding Society (AWS D8.9M:2012) [20]. The tensile shear load of each of the three specimens subjected to the RSW under the same welding conditions was used as the output layer learning data of the ART artificial neural network. The nugget size was measured by cutting the center line of the sample of the RSW.

2.4. Adaptive Resonance Theory

The ART model is characterized in that already learned information is not erased by new information, and even when learning new information, only the corresponding information can be learned. In addition, even if a completely new category of information is entered, learning is performed by setting a new unit, thereby preventing existing learned information from being erased even for information exceeding the storage capacity. Figure 3 shows the structure of the ART network. The ART network consists of F1 layer as input layer, F2 layer as competition layer, gain control to control activation of each layer, and orienting subsystem to check matching with input pattern. The F1 layer and the F2 layer are called short term memory (STM) because they accept and erase data at that time. The up and down weights between F1 layer and F2 layer are called long term memory (LTM) because they memorize information of learned data up to now. First, the current and voltage signals converted into the F1 layer are input. Data input to the F1 layer is calculated by weighting from the F1 layer to the F2 layer, and then goes to the F2 layer. At this time, the F2 layer compares the input data with the previously learned data, and outputs the data that is predicted to be the most similar

among the learned data. The output data is sent back to the F1 layer, and the similarity between the input data and the prediction data is compared in the orienting subsystem. If the degree of similarity is larger than the predetermined value ρ , resonance occurs and the corresponding data is output. If the similarity is smaller than ρ , the learned data is excluded from the search and brought to the other learned data.

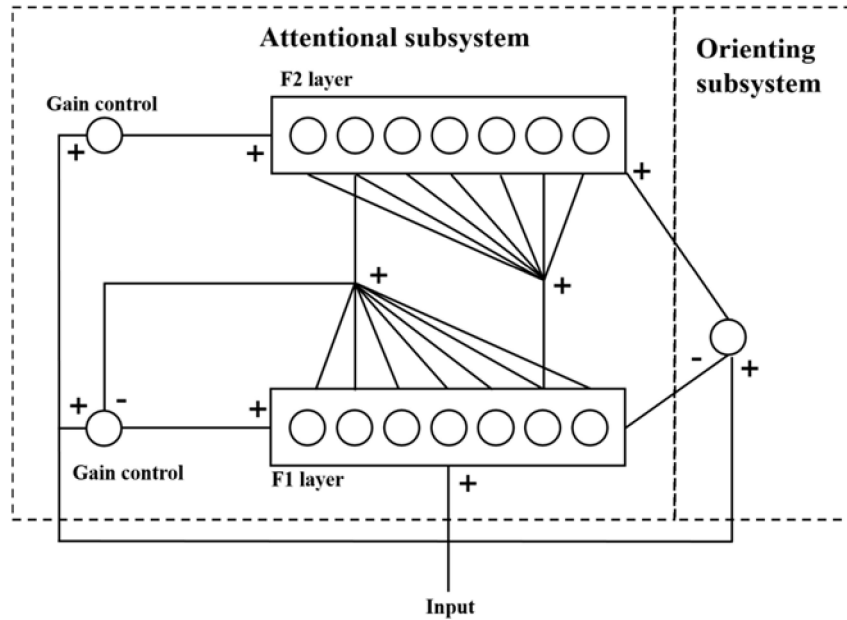


Figure 3. The structure of the adaptive resonance theory (ART) network.

2.5. Conversion of the Input Layer Data for ART Artificial Neural Networks

The input layer information of ART network is a set composed of binary data of 0 and 1. Therefore, input layer signals must be converted into binary data of 0 and 1. Also, these input layer signals are equally divided at a constant interval with respect to the minimum value and the maximum value of the horizontal and the vertical axis is equally divided, thereby two-dimensional plane vectors could be obtained. The welding voltage signal was divided equally between 0 V and 0.05 V, and the welding current signal was divided from 0 kA to 20 kA at intervals of 0.1 kA. For these two signals, the horizontal axis was divided by the time from 0 ms to 300 ms at 1 ms intervals. Accordingly, the signals of the welding current and voltage can be expressed in a two-dimensional plane vector of 100,000 grid lines, respectively. Figure 4a is the mapping of the signal to the two-dimensional plane vector with respect to the welding voltage signal. If the grid where the signal of the welding voltage passes is expressed as 1 and a grid that does not pass a welding voltage signal is expressed as 0, it can be finally expressed as shown in Figure 4c.

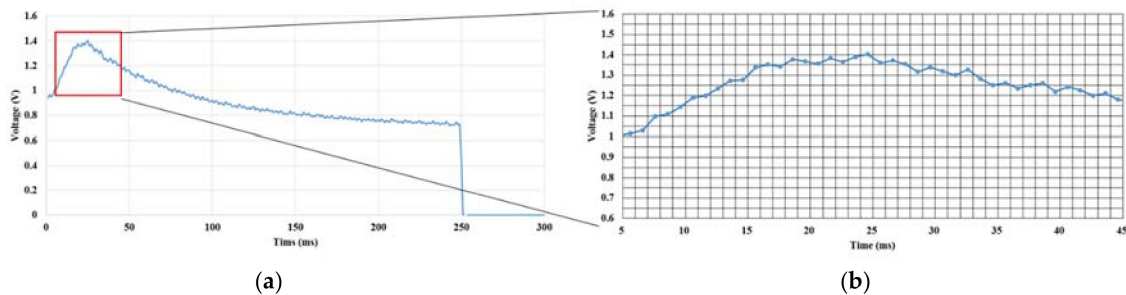


Figure 4. Cont.

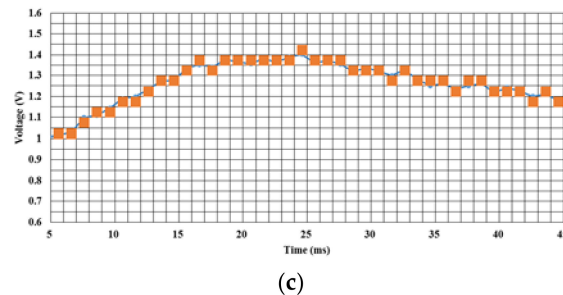


Figure 4. Conversion process of input layer data for ART artificial neural networks in the welding voltage: (a) average welding voltage signal during 1 ms; (b) zoom-in of the average welding voltage signal; and (c) pattern matching result of zoom-in average welding voltage by ART artificial neural networks.

3. Results and Discussion

3.1. Weld Quality of RSW for 780 MPa Grade DP Steel

Figure 5 shows the average welding voltage and welding current signals measured at the RSW between two layers of 780 MPa grade DP steel with a 1.0 mm thickness under the electrode force of 300 kg_f, the welding current of 7 kA and welding time of 333 ms, respectively. These signals were used as the input layer data of the ART artificial neural network. Figure 6 shows the average tensile shear strength and fracture shape of the welds after the tensile test. Also, the measured nugget size and its shape are shown in Figure 7. In this study, the required strength of weld is the 5.9 kN as per the Korean Industrial Standards (KS B0850 B). As shown in Figure 6, when the welding current is 4.0 kA, the required strength was not satisfied at all welding times. For the welding currents of 5.0 and 6.0 kA, tensile shear strength from 7.5 kN to 11 kN was obtained according to the welding time. At welding current of 7.0 kA, tensile shear strength from 12.5 kN to 13.6 kN was shown, and pull-out fracture occurred under all welding times. As shown in Figure 7, the nugget size is from 2.4 mm to 2.6 mm at welding current of 4.0 kA. In the case of welding current with 5.0 kA and 6.0 kA, a nugget size from 3.2 mm to 4.4 mm was obtained according to welding time. At the welding current of 7.0 kA, the nugget sizes were higher than 5.2 mm. As shown in Figures 6 and 7, tensile shear strength and nugget size show no significant difference with increasing welding time at the same welding current, but tend to increase with increasing welding current. Generally, the nugget size is more affected by the welding current than the welding time during RSW of high strength materials. This is related to the increase of contact area during welding by electrode force. The higher strength of the material, the lower initial contact area at the same electrode force, thereby reducing the maximum nugget size. In addition, the contact area by the electrode force during welding is not so large because of the repulsive force due to the high rigidity of the base metal. Therefore, it is advantageous to increase the contact area due to the initial melting by applying a high welding current to obtain a larger nugget size. Therefore, in high-strength materials, the welding current has a greater effect on the change of the nugget size than the welding time. Tensile shear strength is also affected by the nugget size and thus tends to be similar tendency.

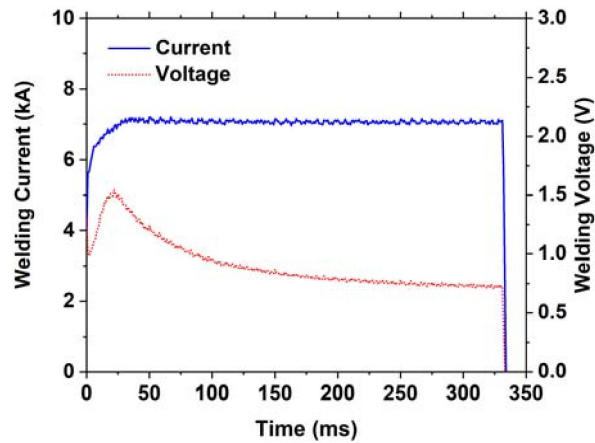


Figure 5. Measured average welding current and voltage signal of 780 MPa grade DP steel with 1.0 mm under the welding current of 7 kA, welding time of 333 ms and electrode force of 300 kg_f.

Welding Time \ Welding Current		4.0 kA	5.0 kA	6.0 kA	7.0 kA
		167 ms			
	Tensile shear strength (kN)	3.8 ± 0.2	7.5 ± 0.2	10.4 ± 0.6	12.5 ± 0.4
250 ms	Fracture shape				
	Tensile shear strength (kN)	4.0 ± 0.2	7.8 ± 0.2	10.7 ± 0.7	13.1 ± 0.6
333 ms	Fracture shape				
	Tensile shear strength (kN)	4.0 ± 0.1	8.2 ± 0.6	11.0 ± 0.7	13.6 ± 0.7

Figure 6. Measured tensile shear strength and fracture shape of the weld with various welding currents and times.

Welding Time \ Welding Current		4.0 kA	5.0 kA	6.0 kA	7.0 kA
		167 ms			
	Nugget size (mm)	2.4	3.2	4.4	5.2
250 ms	Cross section of weld				
	Nugget size (mm)	2.6	3.6	4.4	5.3
333 ms	Cross section of weld				
	Nugget size (mm)	2.5	3.6 mm	4.4	5.2

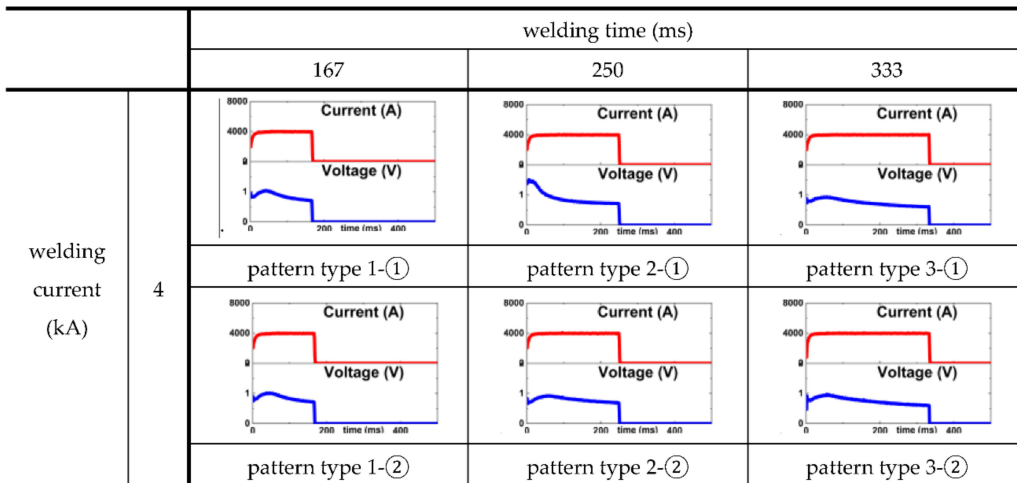
Figure 7. Measured nugget size of the weld with various welding currents and times.

3.2. Optimal Pattern Classification Using ART Artificial Neural Networks

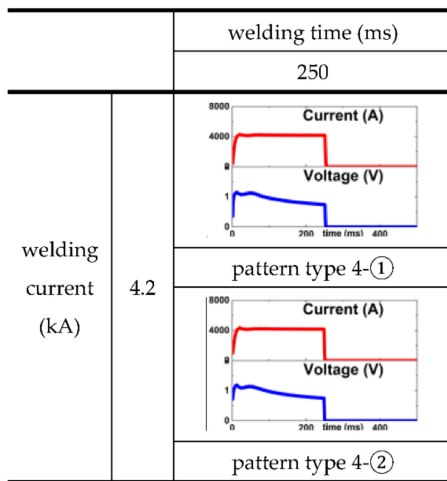
Figure 8 shows the pattern classification of input layer signal for ART artificial neural network according to various welding currents. The prediction principle of ART artificial neural network is to find the most similar pattern among the classified signals by learning the signal pattern of the input layer and the output layer value of the learned signal pattern is used as the predicted value. Therefore, if the output layer variables have values within a certain range, it is very important to group them into the same classification. However, the most important variable affecting this classification is the value of the vigilance parameter (ρ) used in the learning of the ART artificial neural network. When the input data pattern is compared with the clustered pattern that is learned, if the value of the ρ is too high, it is determined that the input data pattern is classified as a pattern of another cluster or that there is no matched pattern. On the other hand, if the value of ρ is too low, even if the input data pattern is greatly changed, it is classified into the same cluster pattern. This results in a large error in the predicted value of the weld quality. Therefore, it is very important to select the appropriate ρ value in order to improve the prediction accuracy of the ART artificial neural network. In order to set the optimal ρ values, the input data of the welding current and voltage were classified using the ART artificial neural network into the cluster data when the ρ are set to 0.7, 0.8, and 0.9, respectively. When ρ is 0.7, the welding current and voltage signals are classified into eight clusters for 15 welding conditions. When ρ is 0.9, 15 welding conditions are divided into 20 clusters. On the other hand, when ρ is 0.8, 15 welding conditions are classified as clusters consisting of 15 welding currents and voltage signals as given. According to the cluster classification result with the change of ρ value, a cluster of the learning data signal is constructed with the $\rho = 0.8$ in this study. Table 3 gives the tensile shear strength, nugget size, and fracture shape for the clustered input signal patterns when the ρ equals 0.8. As shown in Table 3, the tensile shear strength and nugget size vary according to the RSW conditions, and the difference in the patterns of the classified signals becomes clear.

Table 3. Final learning data of ART artificial neural networks at $\rho = 0.8$.

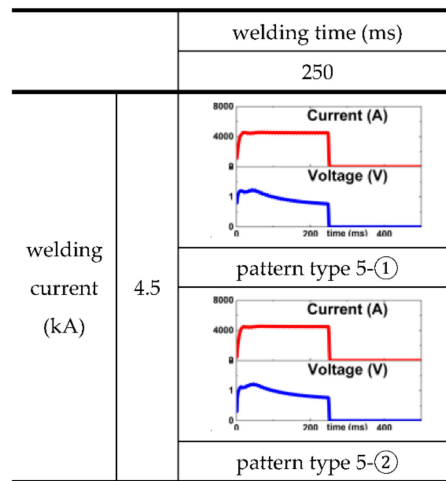
Clusters No.	Tensile Shear Strength (kN)	Nugget Size (mm)	Fracture Shape	CLASSIFIED patterns of Input Signal Parameters
1	3.8	2.4	interfacial	1-①, 1-②
2	4.0	2.5	interfacial	2-①, 2-②
3	4.1	2.6	interfacial	3-①, 3-②
4	5.6	3.0	interfacial	4-①, 4-②
5	6.5	3.1	interfacial	5-①, 5-②
6	7.5	3.2	interfacial	6-①, 6-②
7	7.8	3.5	interfacial	7-①, 7-②
8	8.2	3.6	interfacial	8-①, 8-②
9	9.8	4.0	interfacial	9-①, 9-②
10	10.4	4.2	interfacial	10-①, 10-②
11	10.7	4.3	interfacial	11-①, 11-②
12	11.0	4.4	interfacial	12-①, 12-②
13	12.5	5.2	pull-out	13-①, 13-②
14	13.1	5.3	pull-out	14-①, 14-②
15	13.6	5.4	pull-out	15-①, 15-②



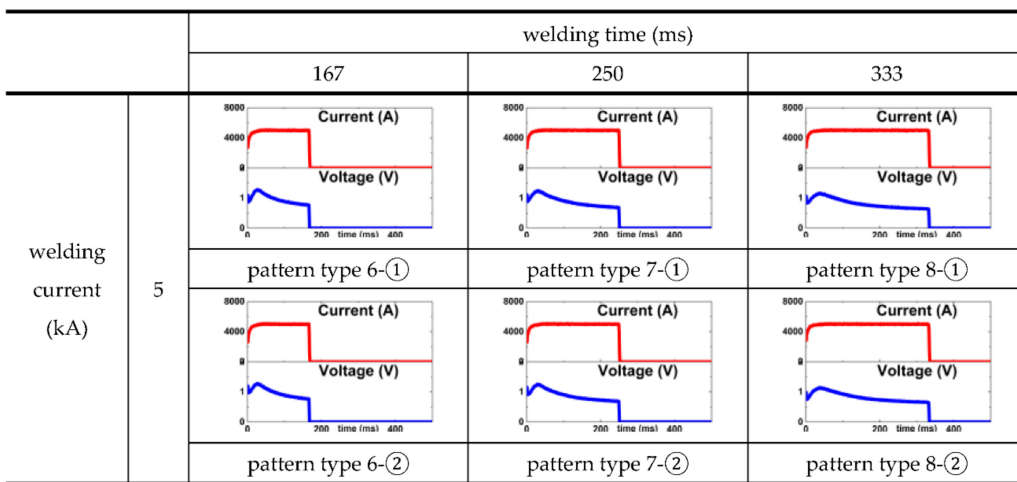
(a)



(b)

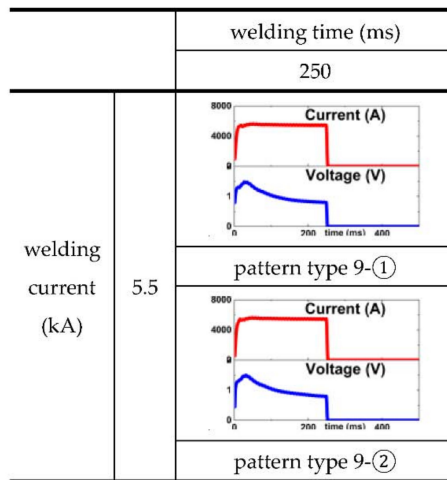


(c)

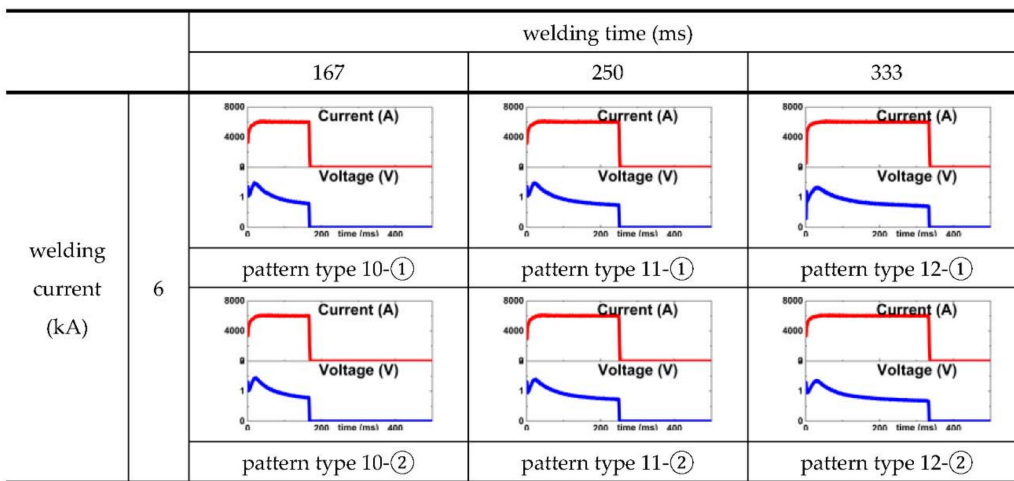


(d)

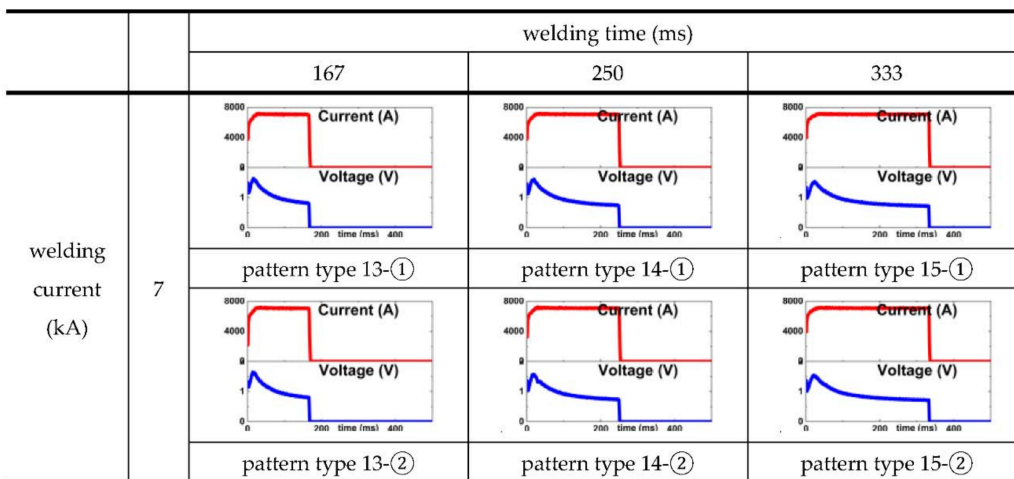
Figure 8. Cont.



(e)



(f)



(g)

Figure 8. Pattern classification of input layer signal for ART artificial neural networks according to the welding current of: (a) 4 kA; (b) 4.2 kA; (c) 4.5 kA; (d) 5 kA; (e) 5.5 kA; (f) 6 kA; and (g) 7 kA.

3.3. Prediction of Weld Quality Using ART Artificial Neural Networks

In order to verify the pattern matching of the new input pattern on the ART network, the welding specimen was prepared for each condition shown in Table 1 and the welding current and voltage signal at that time were measured by the same method as in the previous experiment.

Figure 9 shows a comparison of measured nugget size and tensile shear strength with experimental values using an ART network. The predictive reliability was evaluated by linear regression analysis. The relationship between predicted and experimental results was shown in Figure 9 by the linear equation. And the closer the coefficient of determination (R^2) value is to 1, the higher the predictive reliability. For nugget size and tensile shear strength, R^2 values were 0.9978 and 0.9984, respectively, which means that the predicted value is close to the experimental value. The reason why the prediction accuracy of the tensile strength was slightly higher than the nugget size is that it is difficult to accurately cut the center line in the weld to measure the nugget size and there is an error in the measurement of the length. However, as can be seen from the average prediction results, it is possible to provide useful information for real-time prediction of the nugget size of RSW. In addition, the fracture shape was predicted and compared with the experimental results. In all of the 15 conditions given in Table 3, the predicted results matched the experimental results.

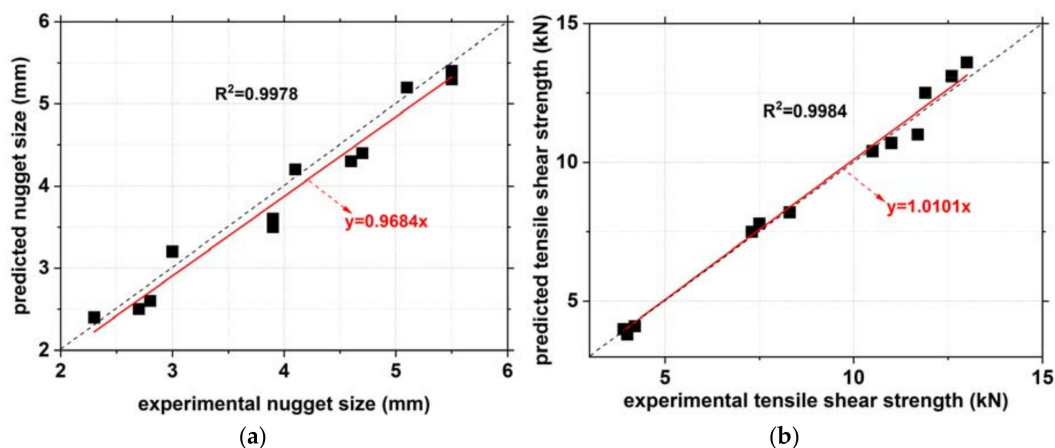


Figure 9. The relationship between the predicted and experimental: (a) nugget size and (b) tensile shear strength.

4. Conclusions

In this study, a model was developed that can predict the quality of RSW using ART artificial neural networks, which is one of the several methods of artificial neural network. The signal information of the welding voltage and current was used as the input parameters of the artificial neural network, and the tensile shear strength, nugget size, and fracture shape of the resistance spot welds were used as output parameters. In ART artificial neural networks pattern classification, it was confirmed that different patterns can be classified under the same welding condition according to the vigilance parameter, ρ . The optimal prediction results were obtained when the vigilance parameter was 0.8. At this time, the predicted values for nugget size and tensile strength using the ART networks were very close to the experimental results. In the prediction of the fracture shape, the accuracy of the prediction was 100%. Based on these results, in the case of predicting the weld quality of RSW in real time, the prediction performance will be excellent when applied to the ART artificial neural networks using the signal of welding voltage and current as input parameters. In addition, it is expected that if welding is carried out under various welding conditions for various types and thicknesses of steel, and the signal of each welding voltage and current is learned, the prediction performance of welding quality will be much better.

Author Contributions: Investigation, H.Y. and J.Y.; Methodology, M.K.; Supervision, M.K., D.K., and Y.-M.K.; Writing—original draft, I.H. and H.Y.; Writing—review and editing, Y.-M.K.

Funding: This work was supported by Technology Innovation Industrial Program funded by the Ministry of Trade, Industry, and Energy (MOTIE, Korea) [Development of the in-line welds quality estimation system and network-based quality control technology in arc and spot welds of ultra-high strength steels for automotive parts assembly].

Acknowledgments: The authors would like to acknowledge the support provided by the Ministry of Trade, Industry, and Energy of the Republic of Korea.

Conflicts of Interest: The authors declare no conflict of interest.

References

1. Schubert, E.; Klassen, M.; Zerner, I.; Walz, C.; Sepold, G. Light-weight structures produced by laser beam joining for future applications in automobile and aerospace industry. *J. Mater. Process. Technol.* **2001**, *115*, 2–8. [[CrossRef](#)]
2. Yamane, K.; Furuhashi, S. A study on the effect of the total weight of fuel and fuel tank on the driving performances of cars. *Int. J. Hydrog. Energy* **1998**, *23*, 825–831. [[CrossRef](#)]
3. Suh, D.W.; Park, S.J.; Lee, T.H.; Oh, C.S.; Kim, S.J. Influence of Al on the microstructural evolution and mechanical behavior of low-carbon, manganese transformation-induced-plasticity steel. *Metall. Mater. Trans. A* **2010**, *41*, 397–408. [[CrossRef](#)]
4. Bouaziz, O.; Allain, S.; Scott, C.P.; Cugy, P.; Barbier, D. High manganese austenitic twinning induced plasticity steels: A review of the microstructure properties relationships. *Curr. Opin. Solid State Mater. Sci.* **2011**, *15*, 141–168. [[CrossRef](#)]
5. Lim, N.S.; Park, H.S.; Kim, S.I.; Park, C.G. Effects of aluminum on the microstructure and phase transformation of TRIP steels. *Metals Mater. Int.* **2012**, *18*, 647–654. [[CrossRef](#)]
6. Kim, H.; Suh, D.W.; Kim, N.J. Fe–Al–Mn–C lightweight structural alloys: A review on the microstructures and mechanical properties. *Sci. Tech. Adv. Mater.* **2013**, *14*, 014205–1–10. [[CrossRef](#)] [[PubMed](#)]
7. Kah, P.; Suoranta, R.; Martikainen, J.; Magnus, C. Techniques for joining dissimilar materials: Metals and polymers. *Rev. Adv. Mater. Sci.* **2014**, *36*, 152–164.
8. Haque, R. Quality of self-piercing riveting (SPR) joints from cross-sectional perspective: A review. *Arch. Civil Mech Eng.* **2018**, *18*, 83–93. [[CrossRef](#)]
9. Ramazani, A.; Mukherjee, K.; Abdurakhmanov, A.; Abbasi, M.; Prahl, U. Characterization of Microstructure and Mechanical Properties of Resistance Spot Welded DP600 Steel. *Metals* **2015**, *5*, 1704–1716. [[CrossRef](#)]
10. Jia, Q.; Liu, L.; Guo, W.; Peng, Y.; Zou, G.; Tian, Z.; Zhou, Y.N. Microstructure and Tensile-Shear Properties of Resistance Spot-Welded Medium Mn Steel. *Metals* **2018**, *8*, 48. [[CrossRef](#)]
11. Russo Spena, P.; Rossi, S.; Wurzer, R. Effects of Welding Parameters on Strength and Corrosion Behavior of Dissimilar Galvanized Q&P and TRIP Spot Welds. *Metals* **2017**, *7*, 534.
12. Tutar, M.; Aydin, H.; Bayram, A. Effect of Weld Current on the Microstructure and Mechanical Properties of a Resistance Spot-Welded TWIP Steel Sheet. *Metals* **2017**, *7*, 519. [[CrossRef](#)]
13. Chabok, A.; van der Aa, E.; De Hosson, J.T.M.; Pei, Y.T. Mechanical behavior and failure mechanism of resistance spot welded DP1000 dual phase steel. *Mater. Des.* **2017**, *124*, 171–182. [[CrossRef](#)]
14. Chen, Z.; Shi, Y.; Jiao, B.; Zhao, H. Ultrasonic nondestructive evaluation of spot welds for zinc-coated high strength steel sheet based on wavelet packet analysis. *J. Mater. Process. Technol.* **2009**, *209*, 2329–2337. [[CrossRef](#)]
15. Lee, S.; Nam, J.; Hwang, W.; Kim, J.; Lee, B. A study on integrity assessment of the resistance spot weld by infrared thermography. *Procedia Eng.* **2011**, *10*, 1748–1753. [[CrossRef](#)]
16. Ji, C.T.; Zhou, Y. Dynamic electrode force and displacement in resistance spot welding of aluminum. *J. Manuf. Sci. Eng.* **2004**, *126*, 605–610. [[CrossRef](#)]
17. El-Banna, M.; Filev, D.; Chinnam, R.B. Online qualitative nugget classification by using a linear vector quantization neural network for resistance spot welding. *Int. J. Adv. Manuf. Technol.* **2008**, *36*, 237–248. [[CrossRef](#)]

18. Zhao, D.; Wang, Y.; Lin, Z.; Sheng, S. An effective quality assessment method for small scale resistance spot welding based on process parameters. *NDT&E Int.* **2013**, *55*, 36–41.
19. Kim, T.; Lee, Y.; Lee, J.; Rhee, S. A study of nondestructive weld quality inspection and estimation during resistance spot welding. *Key Eng. Mater.* **2004**, 270–273, 2338–2344. [[CrossRef](#)]
20. AWS D8.9M. *Test Methods for Evaluating the Resistance Spot Welding Behavior of Automotive Sheet Steel Materials*; American Welding Society (AWS): Miami, FL, USA, 2012.



© 2018 by the authors. Licensee MDPI, Basel, Switzerland. This article is an open access article distributed under the terms and conditions of the Creative Commons Attribution (CC BY) license (<http://creativecommons.org/licenses/by/4.0/>).